Uptake of ^{18}F-Fluorocholine, ^{18}F-Fluoroethyl-L-Tyrosine, and ^{18}F-FDG in Acute Cerebral Radiation Injury in the Rat: Implications for Separation of Radiation Necrosis from Tumor Recurrence

Nicolas Spaeth, DVM[1]; Matthias T. Wyss, MD[1,2]; Bruno Weber, PhD[1]; Stephan Scheidegger, PhD[3]; Amelie Lutz, MD[4]; Jorn Verwey, MS[5]; Ivan Radovanovic, MD[6]; Jens Pahnke, MD[6]; Damian Wild, MD[1]; Gerrit Westera, PhD[2]; Dominik Weishaupt, MD[4]; Dirk M. Hermann, MD[7]; Barbara Kaser-Hotz, DVM[3]; Adriano Aguzzi, MD[6]; and Alfred Buck, MD, MS[1]

[1]PET Center, Division of Nuclear Medicine, University Hospital Zurich, Zurich, Switzerland; [2]Center for Radiopharmaceutical Science of ETH, PSI, and USZ, Paul Scherrer Institute, Villigen, und University Hospital Zurich, Zurich, Switzerland; [3]Section of Diagnostic Imaging and Radio-Oncology, Veterinary Hospital, University Zurich, Zurich, Switzerland; [4]Institute of Diagnostic Radiology, University Hospital Zurich, Zurich, Switzerland; [5]Division of Radiation Medicine, Paul Scherrer Institute, Villigen, Switzerland; [6]Institute of Neuropathology, Department of Pathology, University Hospital Zurich, Zurich, Switzerland; and [7]Department of Neurology, University Hospital Zurich, Zurich, Switzerland

Differentiation between posttherapy radiation necrosis and recurrent tumor in humans with brain tumor is still a difficult diagnostic task. The new PET tracers ^{18}F-fluoro-ethyl-L-tyrosine (FET) and ^{18}F-fluorocholine (*N,N*-dimethyl-*N*-^{18}F-fluoromethyl-2-hydroxyethylammonium [FCH]) have shown promise for improving diagnostic accuracy. This study assessed uptake of these tracers in experimental radiation injury. **Methods:** In a first model, circumscribed lesions were induced in the cortex of 35 rats using proton irradiation of 150 or 250 Gy. After radiation injury developed, uptake of ^{18}F-FET, ^{18}F-FCH, and ^{18}F-FDG was measured using autoradiography and correlated with histology and disruption of the blood–brain barrier as determined with Evans blue. In a second model, uptake of the tracers was assessed in acute cryolesions, which are characterized by the absence of inflammatory cells. **Results:** Mean ^{18}F-FET, ^{18}F-FCH, and ^{18}F-FDG standardized uptake values in the most active part of the radiation lesion and the contralateral normal cortex (in parentheses) were 2.27 ± 0.46 (1.42 ± 0.23), 2.52 ± 0.42 (0.61 ± 0.12), and 6.21 ± 1.19 (4.35 ± 0.47). The degree of uptake of ^{18}F-FCH and ^{18}F-FDG correlated with the density of macrophages. In cryolesions, ^{18}F-FET uptake was similar to that in radiation lesions, and ^{18}F-FCH uptake was significantly reduced. **Conclusion:** Comparison of tracer accumulation in cryolesions and radiation injuries demonstrates that ^{18}F-FET uptake is most likely due to a disruption of the blood–brain barrier alone, whereas ^{18}F-FCH is additionally trapped by macrophages. Uptake of both tracers in the radiation injuries is generally lower than the published uptake in tumors, suggesting that ^{18}F-FET and ^{18}F-FCH are promising tracers for separating radiation necrosis from tumor recurrence. However, the comparability of our data with the literature is limited by factors such as different species and acquisition protocols and modalities. Thus, more studies are needed to settle this issue. Nevertheless, ^{18}F-FCH and ^{18}F-FET seem superior to ^{18}F-FDG for this purpose.

Key Words: radiation necrosis; ^{18}F-fluorocholine; ^{18}F-fluoro-ethyl-L-tyrosine; ^{18}F-FDG; autoradiography

J Nucl Med 2004; 45:1931–1938

Over the last 20 y, PET has become indispensable for evaluating brain tumors. Indeed, diagnosis of brain tumors was the first oncologic application of ^{18}F-FDG PET (*1*). Differentiation of posttherapy radiation necrosis from recurrent tumor remains a challenging diagnostic problem. Correct diagnosis obviously has strong implications for disease management. Attempts with ^{18}F-FDG were only partially successful (*2–5*). One problem is the high intrinsic uptake of ^{18}F-FDG in normal brain cortex, often rendering differentiation of lesions from normal brain difficult. Another is the wide range of ^{18}F-FDG uptake in different brain tumors, leading to an overlap with the degree of uptake in radiation necrosis. Also, MRI and CT cannot reliably separate radiation necrosis from recurrent tumor (*6–8*).

Therefore, the development of more specific radiotracers is a major aim of nuclear medicine research. Radiolabeled choline or amino acid analogs such as ^{18}F-fluorocholine

Received Mar. 10, 2004; revision accepted May 21, 2004.

For correspondence or reprints contact: Alfred Buck, MD, Nuclear Medicine, University Hospital, Rämistrasse 100, 8091 Zürich, Switzerland.

E-mail: fred.buck@usz.ch

(*N,N*-dimethyl-*N*-^{18}F-fluoromethyl-2-hydroxyethylammonium [FCH]) and ^{18}F-fluoro-ethyl-L-tyrosine (FET) seem promising for separating radiation necrosis from tumor recurrence (*9–11*). The ideal tracer for this purpose would reproducibly demonstrate a different accumulation pattern in radiation necrosis from that in tumor, such as no accumulation in radiation necrosis and high accumulation in tumor—a pattern that has been demonstrated for ^{18}F-FET and ^{18}F-FCH.

^{18}F-FET is an amino acid analog that is not metabolized or incorporated into proteins. A specific Na^+-independent amino acid transport system, the L-system, is responsible for high ^{18}F-FET accumulation in tumor cells (*12*). Wester et al. introduced this tracer to clinical research (*13*). Further studies have demonstrated increased uptake of ^{18}F-FET in various brain tumors (*11,14,15*) and lack of uptake by inflammatory tissue (*16,17*). This is important, since radiation necrosis may contain inflammatory cells.

Choline is transported into mammalian cells by specific mechanisms and then phosphorylated by choline kinase. In a further step, choline is metabolized to phosphatidylcholine and incorporated into the cell membrane (*18,19*). The increased choline uptake in tumor cells is explained by upregulation of choline kinase (*20,21*). Initial studies with ^{11}C-choline demonstrated the diagnostic potential of this substance in different tumors (*22–26*). Degrado et al. introduced ^{18}F-FCH for brain tumor imaging (*27*). The major advantage of ^{18}F-labeled compounds, especially in clinical use, is the longer physical half-life of ^{18}F (110 min) than of ^{11}C (20 min). The tumor uptake patterns of ^{11}C-choline and ^{18}F-substituted choline analogs are very similar (*9*). Contrary to ^{18}F-FET, ^{18}F-FCH is accumulated by inflammatory cells (*28*).

The purposes of this study were, first, to assess uptake of ^{18}F-FET, ^{18}F-FCH, and, for comparison, ^{18}F-FDG in experimentally induced acute radiation injury in the rat brain. The tracer uptake pattern was assessed by autoradiography and correlated with histologic findings and disruption of the blood–brain barrier (BBB) as assessed with Evans blue. A second purpose was to evaluate the effect of BBB disruption alone on uptake of ^{18}F-FET and ^{18}F-FCH. For this purpose, ^{18}F-FET and ^{18}F-FCH accumulation was determined in cryolesions, which are characterized by a heavily disrupted BBB but, in contrast to radiation injury, absence of inflammatory cells. Finally, this study assessed the pattern of blood flow in radiation injuries and cryolesions. To this end, perfusion was determined in another group of animals using ^{14}C-iodoantipyrine autoradiography.

MATERIALS AND METHODS

Animals

This study used 35 male Sprague–Dawley rats weighing 250–400 g. All interventions were performed while the animals were under inhalation anesthesia using isoflurane (2–3 vol%, Forene; Abbott Laboratories). The experiments were approved by the local veterinary authorities of the Kanton of Zurich, Switzerland.

Radiopharmaceuticals

4-Iodo-*N*-methyl-^{14}C-antipyrine was obtained from American Radiolabeled Chemicals, Inc. ^{18}F-FDG was obtained from the commercial ^{18}F-FDG production of the University Hospital Zurich. ^{18}F-FET was produced using a method analogous to that of Wester et al. (*13*). ^{18}F-Fluoride (azeotropically dried with 0.7 mL of acetonitrile) was reacted with 10 mg of ethylene glycol-1,2-ditosylate in acetonitrile in the presence of Kryptofix(2.2.2) (Merck) at 110° to give ^{18}F-fluoroethyltosylate, which was purified by reversed-phase high-performance liquid chromatography (HPLC) (LiChrospher 100 RP-18 [Merck], 250 × 10 mm, MeOH/H_2O = 60/40). The product fraction was trapped on a polystyrene cartridge (LiChrolut EN; Merck), dried with nitrogen, and eluted with 0.7 mL of dimethyl sulfoxide into a second vial containing 10 mg of L-tyrosine and 7.5 mg of potassium methylate, where it was reacted for 5 min at 120°. The product was purified by reversed-phase HPLC (LiChrospher 100 RP-18, 10 μm, 250 × 10 mm, EtOH/H_2O/HAc = 8/89.5/2.5, 2.5 g of ammonium acetate per liter). The product peak was sterile filtered into a bottle containing 1 mL of saline and 0.1 mL of phosphate-buffered saline (0.6 mol/L, pH 4). Quality control was by reversed-phase HPLC over LiChrospher 100 RP-18, 5 μm, 250 × 4 mm, eluting with EtOH/H_2O/HAc = 8/89.5/2.5, with 2.5 g of ammonium acetate per liter. Radiochemical purity was >99%. In the ultraviolet trace, ^{18}F-FET was not visible and no quantifiable impurities were visible. Enantiomeric purity was determined by chiral ligand exchange HPLC over a Luna C18 column (250 × 4.6 mm, 5 μm) coated with L-penicillamine chiral selector, eluting with 30% methanol in 5 mmol of aqueous $CuSO_4$ per liter. Starting from L-tyrosine as the substrate, no D-(*R*)-*O*-^{18}F-fluoroethyltyrosine was detected.

^{18}F-FCH was produced by the reaction of ^{18}F-fluoromethyltriflate with diaminoethanol. ^{18}F-Fluoride (azeotropically dried with 2 × 0.7 mL of acetonitrile) was reacted with dibromomethane in acetonitrile in the presence of Kryptofix(2.2.2) at 110° to give ^{18}F-fluorobromomethane (*29*), which was purified over a series of 4 Sep-Pak Plus silica cartridges (Waters). ^{18}F-Fluoromethyltriflate was made by passing ^{18}F-bromofluoromethane over a silver triflate/Graphpac GC column (Alltech Associates Inc.) at 180°. ^{18}F-Fluoromethyltriflate was then used for the *N*-alkylation of 2-dimethylaminoethanol immobilized on a Sep-Pak Plus C-18 cartridge (a solution of 2-dimethylaminoethanol in ethanol [200 μL in 600 μL] was put on the cartridge), to quantitatively yield the desired product. For purification, ^{18}F-FCH was selectively trapped on a Sep-Pak Accel CM cartridge (Waters), washed with water, removed with saline, and, via a sterile filter, added to a patient bottle with 4 mL of saline, 0.5 mL of 10% NaCl, and 70 μL of $NaHCO_3$. Quality control was by HPLC over a cation exchange column (*30*). Supelcosil LC-SCX (Supelco, Inc.), 250 × 4.6 mm, 5 μm, eluting with a 0.15 mol/L concentration of NaH_2PO_4 in water/pyridine (1,000/0.08 v/v), was adjusted to pH 2.37 by 70% H_3PO_4. Radiochemical purity was >99%. In the ultraviolet trace, ^{18}F-FCH was not visible and no quantifiable impurities were visible.

Proton Irradiation

The rats were irradiated with a thin, collimated proton beam of 3-mm diameter at the Facility for Ocular Tumor Treatment (*31*) of the Paul Scherrer Institute. The energy of the protons was adapted to the required penetration depth of the beams or to the Bragg peak position. This position was evaluated using radiographs and CT scans of rats that were of a size typical of the irradiated animals. To ensure that the Bragg peak was at the same location for each

animal, a special holder was constructed. This holder was placed on the patient chair, which could be positioned with high precision. A laser beam, which marked the proton beam, guided the position of the irradiation point. The radiation was delivered as a single dose of 250 (n = 18) or 150 (n = 5) Gy.

MRI

Weekly sequential MRI examinations after the radiation treatment served for detection of radiation necrosis. MRI was performed on a 1.5-T system (Signa CV/i; General Electric Medical Systems). To maximize signal-to-noise ratio, animals were placed with their heads centrally located in a dedicated wrist coil. This coil was chosen because its design provides an optimal signal-to-noise ratio in relation to the relatively small diameter of a rat's skull. The imaging protocol included the following sequences: an unenhanced transaxial T1-weighted spin-echo sequence (repetition time [TR]/echo time [TE], 300 ms/13 ms; slice thickness, 3 mm, without an interslice gap) and a transaxial T2-weighted 3-dimensional fast spin-echo sequence (TR/TE, 3,000/128; slice thickness, 1.5 mm). In addition, the T1-weighted sequence was acquired in the transaxial plane after administration of gadopentetate dimeglumine (Magnevist [Schering AG], 0.1 mmol/kg of body weight) through a tail vein.

Cryolesions

Cryolesions (n = 12) were used as a model of pure BBB disruption without an inflammatory component. They were induced according to the method described by Hermann et al. (*32,33*). A liquid-nitrogen-cooled copper probe with a tip diameter of 2.5 mm and a tip temperature of −150°C was placed stereotactically through a burr hole onto the right parietal dura mater. Then, the probe was lowered another 200 μm to ensure contact with the cortical tissue and was left for 2 min. ^{18}F-FET and ^{18}F-FCH injections followed 30 min later.

Autoradiography with ^{18}F-FET, ^{18}F-FCH, and ^{18}F-FDG

After detection of radiation injuries on MRI, autoradiography was performed (12–20 d after irradiation in the 250-Gy group, 70–80 d in the 150-Gy group). Two hours before tracer injection, Evans blue was injected into a tail vein. Catheters were then placed in the right femoral artery to monitor blood pressure and in the femoral vein to allow intravenous application of the tracers. Fifteen (^{18}F-FCH and ^{18}F-FET) or 45 (^{18}F-FDG) minutes after injection of 150–200 MBq of tracer, the animals were sacrificed using an overdose of pentobarbital. The brain was removed and instantly frozen in cooled isopentane. For quantification, 10-μm brain slices (100-μm slice distance) were placed on a phosphor imaging screen together with ^{14}C standards and left for 240 min. Tritium-sensitive screens (TR2025; Fuji) were used, as their uncoated, thin, sensitive layer yields higher-resolution ^{18}F autoradiographs than do ordinary screens. The data were scanned (BAS 1800 II [Fuji]; pixel size, 50 μm) and converted to kBq/cm^3. For this conversion, the ^{14}C standards had previously been recalibrated using data from a 4-h exposure of 10-μm slices of brain homogenate containing a defined amount of ^{18}F activity.

For quantitative analysis, the activities were then decay corrected to the time of injection. Dividing these values by the amount of injected activity per gram of body weight yielded standardized uptake values (SUVs). Regions of interest were subsequently placed over the areas with highest and average tracer uptake in the lesions and over contralateral cortex.

4-Iodo-*N*-Methyl-^{14}C-Antipyrine Autoradiography for Evaluation of Perfusion

Two rats of each lesion model (n = 4) were injected with 1.85–2.0 MBq of ^{14}C-iodoantipyrine in 1 mL of saline and sacrificed 1 min later. The brain was removed and instantly frozen in chilled isopentane. Brain slices of 10-μm thickness (100-μm slice distance), together with ^{14}C standards, were placed on a phosphor-imaging screen for 24 h.

Histologic Examination and Evans Blue Fluorescence Imaging

Frozen sections 10 μm thick were fixed with 4% formalin and stained with hematoxylin–eosin for morphologic analysis. For Evans blue visualization, slices were fixed with 4% formalin and stained with 4′,6-diamidino-2-phenylindole (Molecular Probes). Images of the Evans blue distribution were then obtained using a fluorescence microscope. To assess the grade of gliosis, the brain slides were immunohistochemically stained with anti–glial fibrillary acidic protein (GFAP) (DAKO) and developed with the EnVision horseradish peroxidase rabbit system (DAKO).

Statistics

Differences in ^{18}F-FCH and ^{18}F-FET uptake in radiation injury and cryolesions were assessed using the Student 2-tailed unpaired t test.

RESULTS

Animals

In the 2 radiation groups, no animal experienced systemic side effects. Only a small oblong area of alopecia on the temporal skin corresponding to the beam line was discovered during the time of observation.

Radiation Injury

Development of Radiation Injury. Intracerebral lesions were detected on the MRI scans 12 and 70 d after irradiation in the 250- and 150-Gy groups, respectively. The diameter of the lesions ranged from 2 to 6 mm independent of the radiation dose.

Typical examples of MRI scans are demonstrated in Figure 1. The lesion was within the cortex of the right

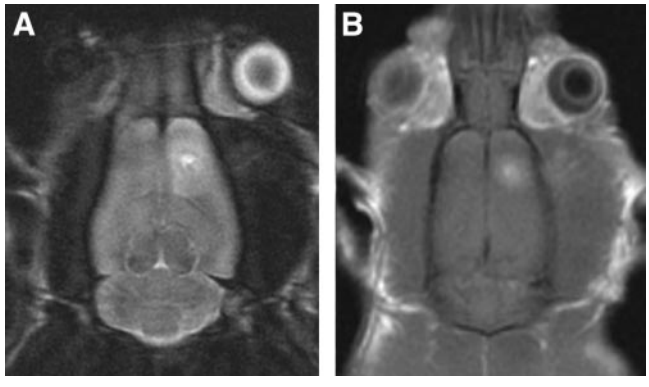

FIGURE 1. Axial MRI scans of rat brain clearly depict radiation lesion in frontoparietal right hemisphere. (A) T2-weighted 3-dimensional fast spin-echo sequence. (B) T1-weighted, gadolinium-enhanced spin-echo scan indicating disruption of the BBB.

frontoparietal region and extended into white matter. It presented as a hyperintense parenchymal signal alteration on the T2-weighted image. On the enhanced T1-weighted image after intravenous administration of gadolinium-diethylenetriaminepentaacetic acid (Magnevist; Schering AG), the entire lesion enhanced slightly, indicating leakage of the BBB.

Histology and Disruption of BBB. Images of a typical radiation injury are shown in Figure 2. Most lesions were characterized by a center of colliquation necrosis (area 1) consisting of cell debris, foamy macrophages, and sometimes calcifications. This center was surrounded by a layer (area 2) consisting of macrophages, reactive astrocytosis (evaluated by GFAP staining), dilated vessels, edema, and, occasionally, small hemorrhages.

Extravasation of Evans blue, indicating BBB disruption, was present in each case. In the example shown in Figure 2, the largest amount of Evans blue accumulated in parts of the necrotic center; smaller amounts were present in the surrounding inflammatory layer (area 2). A similar pattern is found in Figure 3B. In the ^{18}F-FDG example (Fig. 3D), no clear necrotic center was detectable. The small circumscribed area with increased Evans blue accumulation (area 4) did not correspond to the area with highest ^{18}F-FDG uptake (area 3 in Fig. 3C).

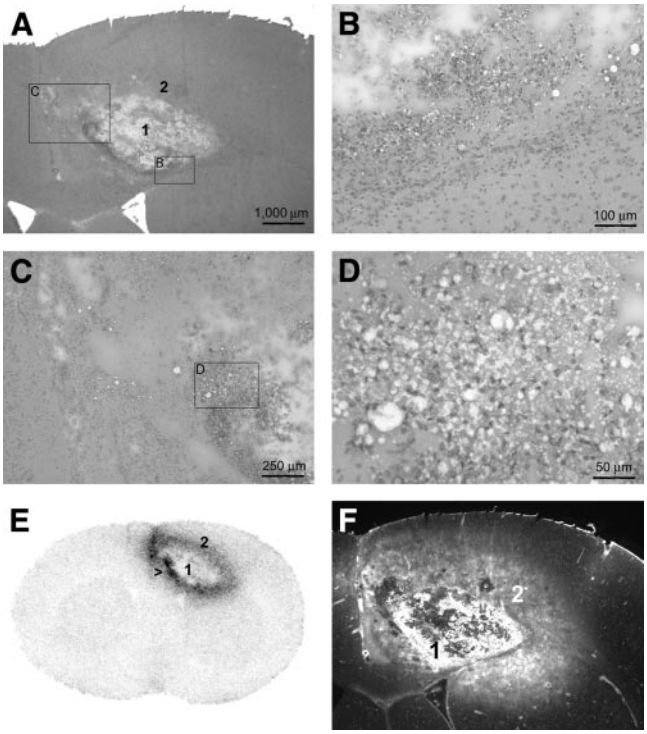

FIGURE 2. Images of radiation injury. (A–D) Hematoxylin- and eosin-stained histologic samples. The overview in panel A demonstrates the necrotic center (area 1) and the surrounding inflammatory layer (area 2). Panels B–D zoom in on layer 2, which is characterized by infiltration of macrophages and reactive astrocytosis. Panel D corresponds to the area with highest uptake of ^{18}F-FCH (arrow in E). The dense infiltrate of macrophages is clearly visible. Panel E depicts uptake of ^{18}F-FCH, which is concentrated in the area adjacent to the central necrosis. (F) Corresponding Evans blue fluorescent scan demonstrates disruption of the BBB.

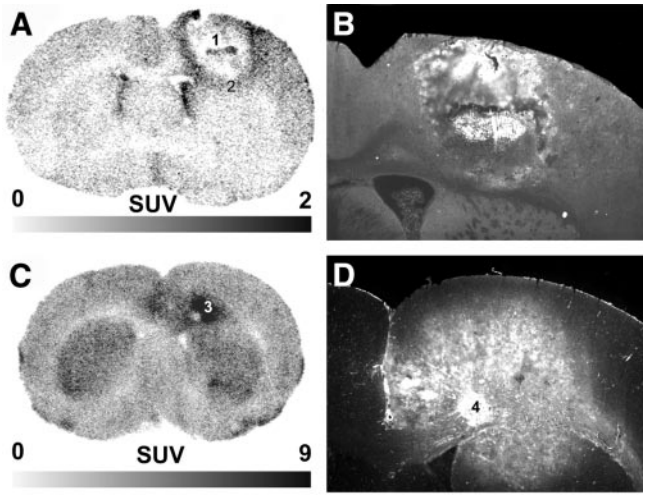

FIGURE 3. Uptake of ^{18}F-FET (A) and ^{18}F-FDG (C), together with the corresponding (B and D, respectively) Evans blue fluorescence scans.

Perfusion Pattern in Radiation Injury. ^{14}C-Iodoantipyrine autoradiography ($n = 2$) demonstrated reduced perfusion in the necrotic center. In the inflammatory layer adjacent to the necrotic center, where ^{18}F-FCH, ^{18}F-FET, and ^{18}F-FDG demonstrated increased uptake, perfusion was similar to that in normal cortex.

Uptake of ^{18}F-FET, ^{18}F-FCH, and ^{18}F-FDG. An autoradiograph demonstrating ^{18}F-FCH uptake is shown in Figure 2E. The highest degree of tracer accumulation was in the inflammatory layer (area 2) surrounding the central necrosis. Examples of ^{18}F-FET and ^{18}F-FDG autoradiographs are shown in Figure 3. ^{18}F-FET accumulation (Fig. 3A) was highest in the inflammatory layer (area 2). In the ^{18}F-FDG example (Fig. 3C), histologic examination revealed no clear necrotic center. The area with the highest ^{18}F-FDG uptake (area 3) was histologically characterized by increased macrophage density.

The SUVs of the various tracers are summarized in Table 1. ^{18}F-FDG displayed by far the highest uptake in the lesions. The SUVs for ^{18}F-FCH and ^{18}F-FET were similar and considerably smaller than for ^{18}F-FDG. The value of L/B (ratio of uptake in lesion to that in contralateral cortex) was highest for ^{18}F-FCH, followed by ^{18}F-FET and ^{18}F-FDG. This ratio to a high degree reflects the differing amounts of tracer accumulation in healthy cortex: least for ^{18}F-FCH, followed by ^{18}F-FET and ^{18}F-FDG.

Cryolesions

Histology and Disruption of BBB. Representative photomicrographs are shown in Figure 4. Cryolesions were characterized mainly by edema. There were no inflammatory cells or reactive astrocytes. Evans blue extravasation is demonstrated in Figure 4A. BBB disruption was present in the entire lesion.

TABLE 1
SUV in Animals with Induced Radiation Necrosis

Animal no.	Tracer	Radiation dose (Gy)	Nec1	Nec2	Ctx	Nec1/Ctx	Nec2/Ctx
1	^{18}F-FCH	250	2.18	1.38	0.58	3.76	2.38
2	^{18}F-FCH	250	2.62	1.43	0.54	4.85	2.65
3	^{18}F-FCH	250	2.18	1.43	0.53	4.11	2.70
4	^{18}F-FCH	250	2.11	1.12	0.54	3.91	2.07
5	^{18}F-FCH	250	2.44	1.25	0.59	4.14	2.12
6	^{18}F-FCH	150	3.22	1.99	0.60	5.37	3.32
7	^{18}F-FCH	150	2.92	1.92	0.86	3.40	2.23
Mean			2.52	1.50	0.61	4.22	2.50
SD			0.42	0.33	0.12	0.67	0.44
8	^{18}F-FET	250	1.25	0.90	0.73	1.71	1.23
9	^{18}F-FET	250	2.13	1.29	1.20	1.78	1.08
10	^{18}F-FET	250	2.64	1.39	1.56	1.69	0.89
11	^{18}F-FET	250	2.52	1.82	1.70	1.48	1.07
12	^{18}F-FET	250	2.40	1.80	1.27	1.89	1.42
13	^{18}F-FET	250	2.44	1.92	1.08	2.26	1.78
14	^{18}F-FET	150	1.77	1.52	1.57	1.13	0.97
15	^{18}F-FET	150	1.98	1.69	1.54	1.29	1.10
Mean			2.27	1.63	1.42	1.64	1.19
SD			0.46	0.34	0.23	0.36	0.29
16	^{18}F-FDG	250	4.82	3.66	4.29	1.12	0.85
17	^{18}F-FDG	250	4.93	4.35	3.62	1.36	1.20
18	^{18}F-FDG	250	6.59	4.48	4.38	1.50	1.02
19	^{18}F-FDG	250	6.50	5.28	5.07	1.28	1.04
20	^{18}F-FDG	250	6.39	3.93	4.24	1.51	0.93
21	^{18}F-FDG	150	8.01	6.11	4.47	1.79	1.37
Mean			6.21	4.64	4.35	1.43	1.07
SD			1.19	0.91	0.47	0.23	0.19

Nec1 = area of highest SUV in necrosis; Nec2 = area of average SUV in necrosis; Ctx = contralateral cortex.

Perfusion in Cryolesions. An example of the perfusion pattern as assessed with ^{14}C-iodoantipyrine is shown in Figure 4B. Perfusion in the lesion was reduced but not absent.

Uptake of ^{18}F-FET and ^{18}F-FCH. Typical ^{18}F-FCH and ^{18}F-FET autoradiographs are shown in Figures 3C and 3D. Accumulation of both tracers was homogeneously increased in the cryolesion, compared with the adjacent and contralateral normal brain tissue.

Table 2 summarizes the SUVs of ^{18}F-FCH and ^{18}F-FET. In lesions, ^{18}F-FET SUVs were on the order of 85% higher than ^{18}F-FCH SUVs. Compared with uptake in radiation injury, ^{18}F-FCH uptake was significantly lower in cryolesions (0.99 ± 0.18 vs. 1.50 ± 0.33, $P = 0.006$). In contrast, ^{18}F-FET accumulation was similar in both types of lesions (1.85 ± 0.34 vs. 1.63 ± 0.34, $P = 0.14$).

DISCUSSION

The main purpose of this study was to evaluate accumulation of the investigated tracers in an acute model of radiation injury so as to assess their ability to separate radiation necrosis from tumor recurrence in humans with brain tumors. All 3 investigated tracers have demonstrated usefulness in the evaluation of brain tumors with PET. ^{18}F-FET and ^{18}F-FCH usually display increased uptake in tumors relative to normal gray matter. Because ^{18}F-FDG is avidly taken up in normal gray matter, one commonly relates tumor uptake to white matter. The ideal tracer to separate tumor recurrence from radiation necrosis would show high uptake in tumors and no uptake in radiation necrosis. That ideal is clearly not met by any of the examined compounds. Three major components determine tracer uptake in lesions. The first is blood flow, which is responsible for tracer delivery. However, the normal or decreased blood flow that is found in areas with increased ^{18}F-FET or ^{18}F-FCH uptake indicates that blood flow is of minor importance. One can therefore concentrate on the other 2 factors: crossing of the BBB, which may be mediated by some regulated process if the BBB is intact or by pure leakage if the BBB has been disrupted, and accumulation in cellular elements. Of note with regard to the latter, a major histologic hallmark of tissue surrounding the necrotic center in radiation injury is macrophage invasion. Previous studies have shown that ^{18}F-FET is not taken up by these cells but is taken up by tissue outside the brain. One of these previous studies addressed ^{18}F-FET uptake in experimentally induced abscesses in the rat thigh muscle (*16*), and the other investigated ^{18}F-FET uptake in murine lymph nodes (*17*). Be-

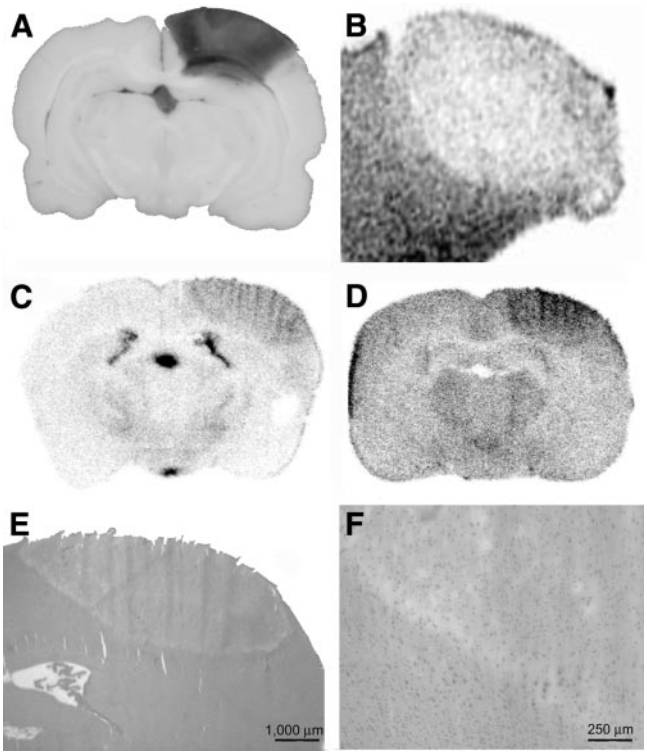

FIGURE 4. Examples of cryolesions. Extravasation of Evans blue, demonstrating disruption of the BBB, is already clearly visible on native images (A). Perfusion in the lesion is decreased relative to that in normal cortex but not absent, as is demonstrated by autoradiography with ^{14}C-iodoantipyrine (B). In contrast, ^{18}F-FCH (C) and ^{18}F-FET (D) uptake is increased in the cryolesion. Hematoxylin–eosin staining (E and F) demonstrate that edema characterizes the histology. There are no signs of inflammatory infiltration.

cause ^{18}F-FET is not taken up by macrophages, the increased uptake in radiation injury is most likely due to leakage of the BBB. This hypothesis was tested in the cryolesions, which served as a model of severe BBB disruption without inflammatory cells. The finding that ^{18}F-FET SUV was similar in radiation injury and cryolesions strongly supports the assumption that ^{18}F-FET uptake in acute radiation injury is indeed driven mainly by leakage across the disturbed BBB. In this context, it is important to note that blood flow in cryolesions was decreased (Fig. 4C). Increased blood flow could have been another reason for the observed increased ^{18}F-FET uptake.

The situation is different for ^{18}F-FCH, which displayed significantly higher uptake in radiation injury than in cryolesions. This finding is consistent with the hypothesis that ^{18}F-FCH uptake in radiation injury is determined by leakage across the BBB and incorporation mainly in macrophages. Because macrophages are missing from cryolesions, ^{18}F-FCH probably diffuses back from tissue into blood in cryolesions but is incorporated into macrophages in radiation injury. That ^{18}F-FCH is indeed incorporated mainly into macrophages and not other cells is suggested by the finding that the areas with highest ^{18}F-FCH uptake coincided with the areas of densest macrophage infiltration. Furthermore, we already demonstrated in a previous study that ^{18}F-FCH is taken up by macrophages (*28*).

There remains the important question of the suitability of the investigated tracers for differentiating radiation necrosis from tumor tissue. We address this question by comparing our data with published data on uptake of ^{18}F-FET, ^{18}F-FCH, and ^{18}F-FDG in brain tumors. However, a direct comparison of our data with the literature is limited by factors such as different acquisition protocols and modalities and interspecies differences.

^{18}F-FET

A direct comparison is possible of our ^{18}F-FET data with the tumor data of Langen et al., who inoculated F98 glioma cells into the brains of 13 CDF Fisher rats and evaluated ^{18}F-FET uptake by autoradiography. They reported a mean L/B of 5.26 ± 1.30 (*34*). This L/B is markedly higher than the values for radiation injury (1.19 ± 0.29, average areas) found by our study.

Weber et al. investigated ^{18}F-FET uptake in 16 patients with various tumors and radiation necrosis (*11*). SUV in the 2 patients with radiation necrosis was 1.1 and 0.8, and L/B was 1.2 and 1.1. These values are smaller than in our study.

TABLE 2
SUVs in Animals with Induced Cryolesions

^{18}F-FCH				^{18}F-FET			
Animal no.	Lesion	Ctx	Lesion/Ctx	Animal no.	Lesion	Ctx	Lesion/Ctx
1	1.29	0.71	1.82	6	1.6	1.10	1.45
2	0.84	0.36	2.33	7	1.52	1.10	1.38
3	0.89	0.45	1.98	8	1.88	1.19	1.58
4	0.97	0.40	2.43	9	1.87	1.21	1.55
5	0.98	0.59	1.66	10	2.38	1.69	1.41
Mean	0.99	0.50	2.04		1.85	1.26	1.47
SD	0.18	0.15	0.33		0.34	0.25	0.09

Ctx = contralateral cortex.

A possible reason is that radiation necrosis in the human study was of a more chronic type. Furthermore, SUVs measured with PET tend to underestimate the true values because of the limited resolution of PET. In the 14 patients with tumors, the L/B was 2.27 ± 0.65. In other studies, this value ranged from 2.0 to 3.3 (*13–15,35,36*). These values are higher than those found by our study, but there is some overlap. With regard to SUV, Weber et al. reported values of 2.67 ± 0.91 and 1.17 ± 0.16 in tumor lesions and normal cortex, respectively. Direct comparison of SUVs in humans and rats is limited, since the magnitude of the SUV depends on the distribution in all tissues that accumulate the tracer, and this distribution may differ between species. In addition, PET SUVs tend to be too small. These factors may be why SUVs in normal cortex were 18% smaller in the human study of Weber et al. than in our animal study. Considering all the available data, and especially the rat study by Langen et al. (*34*), ^{18}F-FET seems promising for separating radiation necrosis from tumor tissue.

Radiolabeled Choline Analogs

For ^{18}F-FCH, the comparison of our data with the literature is less conclusive, since no data are available on ^{18}F-FCH uptake in a rat model of brain tumor. Shinoura et al. measured ^{11}C-choline uptake in C6 glioma cells implanted under the skin of rats. Tumor uptake was 3- to 4-fold higher than brain uptake (*26*). This is higher than the L/B ratio of 2.50 ± 0.44 found by our study. Although Shinoura et al. used ^{11}C-choline, the data should at least in part be comparable, since Hara described similar uptake characteristics for ^{11}C-choline and ^{18}F-labeled choline compounds (*9*). Some data are available from human studies. Degrado et al. also used ^{18}F-FCH and reported an L/B of 10.0 in a single patient with recurrent anaplastic astrocytoma (*27*). Using another ^{18}F-labeled choline analog, ^{18}F-fluoroethyl-dimethyl-2-hydroxyethylammonium, Hara et al. found an L/B in the range of 12–21 for high-grade gliomas (n = 8) and 0–4.8 for grade II astrocytomas (n = 2) (*10*). Ohtani et al. investigated ^{11}C-choline uptake in 20 patients with different brain tumors and calculated tumor–to–white matter ratios in the range of 0.98–29.10 (*37*). The above studies indicate that ^{18}F-FCH in the radiation injury of our study is generally lower than in tumors. However, more studies using ^{18}F-FCH in tumors are needed to settle the issue.

^{18}F-FDG

In our study, accumulation of ^{18}F-FDG in radiation injury was generally on the same order as accumulation in normal cortex (mean L/B = 1.07 ± 0.19, average regions). For comparison, a rat study of Takeda et al. showed a maximum ^{14}C-FDG L/B of approximately 1.2 in intracerebral C6 gliomas (*38*). This is in the same range as the ^{18}F-FDG uptake in our study and leads to the conclusion that ^{18}F-FDG is of questionable suitability for separating radiation necrosis from tumor.

General Remarks

Some differences between our model and human studies are important to mention. The dose and type of irradiation (single dose, 150–250 Gy) used in our study differ from those used on humans. In addition, our model represents acute radiation injury. In humans, a more chronic phase of radiation injury is seen, referred to in the clinical literature as radiation necrosis. In radiation necrosis, the accumulation of inflammatory cells and degree of BBB disruption is probably less pronounced than in acute radiation injury. Typical alterations include wall thickening, fibrinoid necrosis, hyalinization of the vessel walls, and extensive gliosis adjacent to the necrotic focus (*39*). Therefore, uptake of all investigated tracers in such lesions is likely to be smaller. The low ^{18}F-FET uptake found by Weber et al. (*11*) for 2 cases of human radiation necrosis points in this direction. A lower uptake would increase the specificity for diagnosing radiation necrosis, especially for ^{18}F-FET and ^{18}F-FCH. However, more studies on ^{18}F-FCH and ^{18}F-FET uptake in chronic radiation lesions are needed to settle this issue.

CONCLUSION

The presented data elucidate the mechanism of ^{18}F-FET and ^{18}F-FCH uptake by acute radiation injuries and acute cryolesions. ^{18}F-FET uptake is determined mainly by disruption of the BBB, whereas ^{18}F-FCH is additionally trapped by inflammatory cells. Uptake of both tracers in radiation injuries was generally lower than published uptake values in tumors, suggesting that ^{18}F-FET and ^{18}F-FCH are promising for separating radiation necrosis from tumor recurrence. However, the comparability of our data with the literature is limited by factors such as differences in species and acquisition protocols and modalities. Thus, more studies are needed to settle this issue. Nevertheless, ^{18}F-FCH and ^{18}F-FET seem superior to ^{18}F-FDG for this purpose.

ACKNOWLEDGMENTS

This study was supported by the Radium-Stiftung and the OPO Stiftung in Zurich. The authors thank Hans Blattmann and Gustav K. von Schulthess for valuable discussions, Emanuel Egger for support with the proton gantry, Kerstin Goepfert for assistance with MRI, Susanne Hess for superb photographic work, and Tibor Cservenyak and Rolf Hesselmann for tracer production.

REFERENCES

1. Di Chiro G, DeLaPaz RL, Brooks RA, et al. Glucose utilization of cerebral gliomas measured by [^{18}F] fluorodeoxyglucose and positron emission tomography. *Neurology.* 1982;32:1323–1329.
2. Chao ST, Suh JH, Raja S, Lee SY, Barnett G. The sensitivity and specificity of FDG PET in distinguishing recurrent brain tumor from radionecrosis in patients treated with stereotactic radiosurgery. *Int J Cancer.* 2001;96:191–197.
3. Kahn D, Follett KA, Bushnell DL, et al. Diagnosis of recurrent brain tumor: value of ^{201}Tl SPECT vs ^{18}F-fluorodeoxyglucose PET. *AJR.* 1994;163:1459–1465.
4. Ricci PE, Karis JP, Heiserman JE, Fram EK, Bice AN, Drayer BP. Differentiating recurrent tumor from radiation necrosis: time for re-evaluation of positron emission tomography? *AJNR.* 1998;19:407–413.
5. Thompson TP, Lunsford LD, Kondziolka D. Distinguishing recurrent tumor and

radiation necrosis with positron emission tomography versus stereotactic biopsy. *Stereotact Funct Neurosurg.* 1999;73:9–14.
6. Del Sole A, Falini A, Ravasi L, et al. Anatomical and biochemical investigation of primary brain tumours. *Eur J Nucl Med.* 2001;28:1851–1872.
7. Dooms GC, Hecht S, Brant-Zawadzki M, Berthiaume Y, Norman D, Newton TH. Brain radiation lesions: MR imaging. *Radiology.* 1986;158:149–155.
8. Mikhael MA. Radiation necrosis of the brain: correlation between computed tomography, pathology, and dose distribution. *J Comput Assist Tomogr.* 1978;2:71–80.
9. Hara T. ^{11}C-Choline and 2-deoxy-2-[^{18}F]fluoro-D-glucose in tumor imaging with positron emission tomography. *Mol Imaging Biol.* 2002;4:267–273.
10. Hara T, Kondo T, Kosaka N. Use of ^{18}F-choline and ^{11}C-choline as contrast agents in positron emission tomography imaging-guided stereotactic biopsy sampling of gliomas. *J Neurosurg.* 2003;99:474–479.
11. Weber WA, Wester HJ, Grosu AL, et al. O-(2-[^{18}F]fluoroethyl)-L-tyrosine and L-[methyl-^{11}C]methionine uptake in brain tumours: initial results of a comparative study. *Eur J Nucl Med.* 2000;27:542–549.
12. Heiss P, Mayer S, Herz M, Wester HJ, Schwaiger M, Senekowitsch-Schmidtke R. Investigation of transport mechanism and uptake kinetics of O-(2-[^{18}F]fluoroethyl)-L-tyrosine in vitro and in vivo. *J Nucl Med.* 1999;40:1367–1373.
13. Wester HJ, Herz M, Weber W, et al. Synthesis and radiopharmacology of O-(2-[^{18}F]fluoroethyl)-L-tyrosine for tumor imaging. *J Nucl Med.* 1999;40:205–212.
14. Baum RP, Calcagni M, Dimitrakopoulou-Strauss A, Strauss LG. Pharmakokinetic analysis of O-2-[^{18}F]fluorethyl-L-tyrosin (^{18}F-FET) by dynamic PET in the differential diagnosis of malignant gliomas [abstract]. *J Nucl Med.* 2003;44(suppl):63P.
15. Cheon GJ, Ahn SH, Cho YS, et al. Correlation of ^{18}F-FET uptake and histologic grades of primary brain tumors [abstract]. *J Nucl Med.* 2003;44(suppl):367P.
16. Kaim AH, Weber B, Kurrer MO, et al. (18)F-FDG and (18)F-FET uptake in experimental soft tissue infection. *Eur J Nucl Med Mol Imaging.* 2002;29:648–654.
17. Rau FC, Weber WA, Wester HJ, et al. O-(2-[(18)F]Fluoroethyl)-L-tyrosine (FET): a tracer for differentiation of tumour from inflammation in murine lymph nodes. *Eur J Nucl Med Mol Imaging.* 2002;29:1039–1046.
18. Kennedy EP, Weiss SB. The function of cytidine coenzymes in the biosynthesis of phospholipids. *J Biol Chem.* 1956;222:193–214.
19. Zeisel SH. Dietary choline: biochemistry, physiology, and pharmacology. *Annu Rev Nutr.* 1981;1:95–121.
20. Haeffner EW. Studies on choline permeation through the plasma membrane and its incorporation into phosphatidyl choline of Ehrlich-Lettre-ascites tumor cells in vitro. *Eur J Biochem.* 1975;51:219–228.
21. Katz-Brull R, Degani H. Kinetics of choline transport and phosphorylation in human breast cancer cells: NMR application of the zero trans method. *Anticancer Res.* 1996;16:1375–1380.
22. Hara T, Inagaki K, Kosaka N, Morita T. Sensitive detection of mediastinal lymph node metastasis of lung cancer with ^{11}C-choline PET. *J Nucl Med.* 2000;41:1507–1513.
23. Hara T, Kosaka N, Kishi H. PET imaging of prostate cancer using carbon-11-choline. *J Nucl Med.* 1998;39:990–995.
24. Hara T, Kosaka N, Shinoura N, Kondo T. PET imaging of brain tumor with [methyl-^{11}C]choline. *J Nucl Med.* 1997;38:842–847.
25. Kobori O, Kirihara Y, Kosaka N, Hara T. Positron emission tomography of esophageal carcinoma using (11)C-choline and (18)F-fluorodeoxyglucose: a novel method of preoperative lymph node staging. *Cancer.* 1999;86:1638–1648.
26. Shinoura N, Nishijima M, Hara T, et al. Brain tumors: detection with C-11 choline PET. *Radiology.* 1997;202:497–503.
27. DeGrado TR, Baldwin SW, Wang S, et al. Synthesis and evaluation of (18)F-labeled choline analogs as oncologic PET tracers. *J Nucl Med.* 2001;42:1805–1814.
28. Wyss MT, Weber B, Honer M, et al. ^{18}F-choline in experimental soft tissue infection assessed with autoradiography and high-resolution PET. *Eur J Nucl Med Mol Imaging.* 2004;31:312–316.
29. Bergman J, Eskola O, Lehikoinen P, Solin O. Automated synthesis and purification of [^{18}F]bromofluoromethane at high specific radioactivity. *Appl Radiat Isot.* 2001;54:927–933.
30. Vassiliev D, Krasikova R, Kuznetsova O, Fedorova O, Nader M. Simple HPLC method for the detection of N,N-dimethylaminoethanol in the preparation of [N-methyl-^{11}C]choline. *Eur J Nucl Med.* 2003;30(suppl):S311.
31. Egger E, Zografos L, Perret C. Proton beam irradiation of choroidal melanomas at PSI: technique and results. In: Sagerman RH, Alberti WE, eds. *Medical Radiology: Diagnostic Imaging and Radiation Oncology—Radiotherapy of Intraocular and Orbital Tumors.* New York, NY: Springer-Verlag; 1993:57–72.
32. Hermann DM, Kilic E, Kugler S, Isenmann S, Bahr M. Adenovirus-mediated glial cell line-derived neurotrophic factor (GDNF) expression protects against subsequent cortical cold injury in rats. *Neurobiol Dis.* 2001;8:964–973.
33. Hermann DM, Mies G, Hossmann KA. Effects of a traumatic neocortical lesion on cerebral metabolism and gene expression of rats. *Neuroreport.* 1998;9:1917–1921.
34. Langen KJ, Jarosch M, Muhlensiepen H, et al. Comparison of fluorotyrosines and methionine uptake in F98 rat gliomas. *Nucl Med Biol.* 2003;30:501–508.
35. Pauleit DO, Floeth F, Hamacher K, et al. Influence of blood-brain barrier disruption on FET uptake in cerebral gliomas [abstract]. *J Nucl Med.* 2003;44(suppl):244P.
36. Poepperl G, Goetz C, Rachinger W, et al. Value of [^{18}F]fluoroethyltyrosine PET for the diagnosis of recurrent malignant astrocytomas [abstract]. *J Nucl Med.* 2003;44(suppl):166P.
37. Ohtani T, Kurihara H, Ishiuchi S, et al. Brain tumour imaging with carbon-11 choline: comparison with FDG PET and gadolinium-enhanced MR imaging. *Eur J Nucl Med.* 2001;28:1664–1670.
38. Takeda A, Tamano H, Enomoto S, Oku N. Zinc-65 imaging of rat brain tumors. *Cancer Res.* 2001;61:5065–5069.
39. The pathology of central nervous system radiation injury. In: Gutin PH, Leibel SA, Sheline GE, eds. *Radiation Injury to the Nervous System.* New York, NY: Raven Press; 1991:191–208.